Original papers

CFD modelling of an animal occupied zone using an anisotropic porous medium model with velocity depended resistance parameters

E. Moustapha Doumbia [a,*], David Janke [a], Qianying Yi [a], Thomas Amon [a,b], Martin Kriegel [c], Sabrina Hempel [a]

[a] Leibniz Institute for Agricultural Engineering and Bioeconomy, Department of Engineering for Livestock Management, Potsdam, Germany
[b] Institut of Animal Hygiene and Environmental Health, Department of Veterinary Medicine, Freie Universität Berlin, Germany
[c] Hermann-Rietschel-Institut, Chair of Building Energy Engineering, Technische Universität Berlin, Germany

ABSTRACT

The airflow in dairy barns is affected by many factors, such as the barn's geometry, weather conditions, configurations of the openings, cows acting as heat sources, flow obstacles, etc. Computational fluids dynamics (CFD) has the advantages of providing detailed airflow information and allowing fully-controlled boundary conditions, and therefore is widely used in livestock building research. However, due to the limited computing power, numerous animals are difficult to be designed in detail. Consequently, there is the need to develop and use smart numerical models in order to reduce the computing power needed while at the same time keeping a comparable level of accuracy.

In this work the porous medium modeling is considered to solve this problem using Ansys Fluent. A comparison between an animal occupied zone (AOZ) filled with randomly arranged 22 simplified cows' geometry model (CM) and the porous medium model (PMM) of it, was made. Anisotropic behavior of the PMM was implemented in the porous modeling to account for turbulence influences. The velocity at the inlet of the domain has been varied from 0.1 m s^{-1} to 3 m s^{-1} and the temperature difference between the animals and the incoming air was set at 20 K. Leading to Richardson numbers Ri corresponding to the three types of heat transfer convection, i.e. natural, mixed and forced convection. It has been found that the difference between two models (the cow geometry model and the PMM) was around 2% for the pressure drop and less than 6% for the convective heat transfer. Further the usefulness of parametrized PMM with a velocity adaptive pressure drop and heat transfer coefficient is shown by velocity field validation of an on-farm measurement.

1. Introduction

Indoor air flow pattern and temperature are among the key parameters to evaluate livestock housing with regard to animal welfare and environmental requirements. But the distribution of air speed and temperature inside a building is not homogeneous, where local deviations are considerably affected by the livestock itself (Gebremedhin and Wu, 2005; Bustos-Vanegas et al., 2019; Wang et al., 2018). Difficulties exist in measuring climate conditions inside the animal occupied zone (AOZ) because of the temporal and spatial fluctuation nature of the climate itself and the possible disturbance of animals to measurement instruments (Saha et al., 2014; Kiwan et al., 2012). In consequence, computational fluids dynamics (CFD) methods are applied as a support tool with increasing frequency in agricultural research to model the interior air flow in barns. Due to the theoretically unlimited spatial and temporal resolution and the defined boundary conditions, those simulations are an optimal complement for measurements and permit deep insights into the development of air flow patterns. Model complexity and accuracy depend on the computational power and the chosen parametrizations of unresolved processes. Particularly in the vicinity of sharp edges in the geometry the resolution of the computation mesh must be very fine to ensure convergence of the numerical integration schemes and acceptable accuracy of the simulations (Saha et al., 2014; Lanfrit, 2005). On the other hand, very detailed models can require unreasonably long computation times. To overcome this problem, parametrization of certain effects and/or processes is a common approach.

In this context, porous media modeling is a technique that has been used in many fields in order to replace complex geometries. For example fishing nets in the fishing industry (Patursson et al., 2010), soil in

---

Nomenclature

α	Power coefficient, here 0.16 from our wind tunnel measurement
ΔT_{log}	$\frac{T_{out} - T_{in}}{ln \frac{T_{cow} - T_{out}}{T_{cow} - Tin}}$, K
$\dot{m}$	Mass flow rate, kg s^{-1}
$\frac{\Delta P_i}{\Delta x_i}$	Pressure drop per unit length, Pa m^{-1}
μ	Air dynamic viscosity, pa s
ρ	Air density, kg m^{-3}
A_s	Interface area between cows and air, m^2
A_{fs}	Interfacial area density, i.e. ratio between the solid/fluid interface area and the fluid volume, m^{-1}
AER	Air exchange rate of the volume V_{AER}, h^{-1}
C_p	Cow surface specific heat capacity, J kg^{-1} K^{-1}
CM	cows model
D	Viscous resistance matrix, m^{-2}
F	Inertial resistance matrix, m^{-1}
Gr	Grashof number
h_{cows}	Heat transfer coefficient between cows and air, W m^{-2} K^{-1}
h_{fs}	Interstitial heat transfer coefficient between the fluid/solid interface, W m^{-2} K^{-1}
PMM	Porous medium model
Q_{conv}	Convective heat transfer, W
Re	Reynolds number
T_f	Fluid temperature, here: inlet air temperature, K
T_s	Solid temperature, here: cow surface temperature, K
T_{in}	Inlet fluid temperature, K
T_{out}	Outlet fluid temperature, K
u	Velocity, m s^{-1}
U_{ref}	Reference velocity at the reference height y_{ref}, m
V	Sum of volume flow entering in V_{AER}, m^3 s^{-1}
V_{AER}	Considered volume for AER evaluation, m^3
y_{ref}	Reference height at which the velocity = U_{ref}, here H/2, m s^{-1}

---

geothermal application (Zhou et al., 2019), plants and trees in agriculture (Tiwary and Morvan, 2006), or packed bed for reactors (Ahmadi and Sefidvash, 2018). In livestock buildings, Yin et al. (2016), Rong et al. (2010), for example, used porous media as replacement of slatted floors to investigate air flow and ammonia emission. In this work, however, the porous media was considered as isotropic in the three main directions and the heat transfer was not considered. In addition, the porous media modeling has also been used to model the animals themselves as flow obstacles in non darcy flows (Mendes et al., 2014) and also as heat source (Bjerg, 2011). Bjerg (2011) used anisotropic porous media, which resistance parameters have been determined based on 3D detailed geometries, in order to model AOZ of pigs for the study of the air quality while taking into account heat release from the animals. However, the accuracy of porous medium as replacement of 3D detailed geometries was not addressed in that study.

Since a usual barn contains hundreds of cattle, modeling every single of them would require a massive amount of computing power. Thus the porous media modeling for the AOZ can be very valuable to drastically reduce the simulation time.

So far, the implementation of porous medium modeling as replacement of modeled animals in dairy barns was almost limited to effects in the main flow direction. This is a strong simplification since air flow in naturally ventilated barns must be considered as turbulent flow, where diverse three dimensional air directions are involved inside, even with a one dimensional direction wind inlet. In previous studies, Doumbia et al. (2019) and Saha et al. (2014) have shown that the flow even inside an empty barn is turbulent. Furthermore in his study Bustos-Vanegas et al. (2019) has demonstrated how the pressure drop of the AOZ changed depending on the incoming velocity angle, showing the anisotropic character of the AOZ. Based on those observations, with the goal to reach higher accuracies, we decided to pay particular attention on the anisotropic character of AOZ as well as the velocity-dependency of the flow resistance and the heat transfer coefficient of the AOZ. We tested the following hypothesis: the adaption of the flow resistance parameters in both air direction and air velocity and the heat transfer coefficient accordingly improves the approximation of pressure drop and heat transfer in the porous media modeling.

Our work presents a methodological approach to reproduce the flow created by the animals shape by best possible implementing the pressure drop and the heat transfer in the porous medium. The first part deals with the modeling of the pressure drop. Particularities of the porous medium are introduced and the characteristic viscous and inertial coefficients are determined. The second part concerns the reproduction of

the heat transfer by the porous medium. A heat transfer coefficient is obtained for the studied AOZ as a function of the velocity. In the third part the fully resolved AOZ and the corresponding porous medium are compared in a large domain for the three types of convection (natural, mixed and forced). And the last part presents a case validation against on farm measurement using simulation with only PMMs.

2. Development and evaluation method of the models

2.1. Setup of computational fluid dynamics simulations

The modeled animal occupied zone (AOZ, height $H = 1.6$ m, width $W = 4.9$ m, length $L = 10.8$ m) has been filled with cows with a density of 2.4 m^2 cow^{-1}, according to ATB's experimental barn in Dummerstorf, Germany. It is made of 22 cows extracted from the barn AOZ arrangement plan. A 60% lying cows, 40% standing cows configuration has been chosen since most of the time cows are lying (16–18 h per day) (The Danish Agricultural Advisory Center, 2001). The angle position of the cows is random (with 15, 30 and 90 degree). The 3D cow model is a simplified version of a 3D cow as used by Bustos-Vanegas et al. (2019), see Fig. reffig1(b). The simplified cow geometry has been chosen for this study because of its costs and benefits in terms of computational effort and accuracy. It permits the use of less dense grids (resulting in faster computation), while Mondaca and Choi (2015) have shown that the simplified geometry resulted in almost identical results in flow patterns and heat transfer analysis when compared with a highly detailed polygon model of a cow.

The K-Omega SST has been chosen as turbulence model, since the study of Stamou and Katsiris (2006) has shown that this turbulence model has better accuracy with the measurement for velocity and temperature compared to the standard K-Epsilon turbulence model. The suitability of this turbulence model for natural convection dominating flows was confirmed by Defraeye et al. (2012). A mesh inflation has been set at the cows' surface in order to obtain a wall Y$^+$ smaller than one. The meshing has been done with tetrahedral cells in Ansys meshing and then set to polyhedral in Ansys Fluent (version R2 2019). This Fluent-technique improves the stability and the convergence of the solution while reducing the total number of cells by merging together the tetrahedral cells. All the simulations have been run in steady state (time independent). The pressure velocity coupling scheme has been set to "coupled", getting better convergence from our experience. The spatial discretization schemes have been kept standard which means second order upwind for the momentum and the energy, first order upwind for

the turbulent kinetic energy and the specific dissipation rate, second order for the pressure for the cow model (CM) case but "PRESTO!" for the porous medium model (PMM) case, as suggested by Fluent user guide (ANSYS, 2019). Convergence is considered as being achieved when the residuals are below 10^{-3} overall and below 10^{-5} for energy (ANSYS, 2019).

In order to be sure that the simulations are unaffected by the mesh density, a grid independence study has been performed. A mesh refinement sub-domain has been added, where the cell size is half of the domain cell size, see Fig. 1(c). The dimensions of the refinement sub-domain follows the recommendations of Lanfrit (2005), see Fig. 1(a). The results of the grid independence study are summarized in Table 1. The study has been done when the air is flowing in the x main direction, see chapter 2.2. The relative difference of the pressure drop $\left(\left|\Delta p_{cell\ size} - \Delta p_{next\ coarser\ cell\ size}\right| \cdot \Delta p_{cell\ size}^{-1} \cdot 100\right)$ and of the heat transfer coefficient $\left(\left|\Delta h_{cell\ size} - \Delta h_{next\ coarser\ cell\ size}\right| \cdot \Delta h_{cell\ size}^{-1} \cdot 100\right)$ have been evaluated. It appears that the relative differences between the mesh sizes are the smallest for the cell size couple (domain and refinement box) 0.8–0.4 m and 0.6–0.3 m $\left(\left|\Delta p_{(0.6-0.3)} - \Delta p_{(0.8-0.4)}\right| \cdot \Delta p_{(0.6-0.3)}^{-1} \cdot 100 = 2.66\% \text{ and } \left|\Delta h_{(0.6-0.3)} - \Delta h_{(0.8-0.4)}\right| \cdot \Delta h_{(0.6-0.3)}^{-1} \cdot 100 = 0.05\%\right)$. Hence the cell size couple 0.8–0.4 m has been used for the rest of the study.

2.2. Pressure drop modelling

The porous media model adds a momentum source term S_i (i represents the x, y or z direction of the Cartesian coordinate) to the governing equation.

Table 1
Grid convergence study. The two Rel. Diff. parameters highlights the relative change of the simulation from the next coarser resolution to the current one.

Domain cell size	Ref. cell size	Total cell number	ΔP_x	Rel. Diff. Δp_x	h	Rel. Diff(h)
m	m	(–)	P·m^{-1}	%	W·m^{-2}·K^{-1}	%
0.6	0.3	2073828	0.1533	2.66	8.841	0.05
0.8	0.4	1934122	0.1493	3.33	8.846	0.29
1.4	0.7	1872760	0.1545	1.11	8.872	0.43
2	1	1869281	0.1528		8.834	

$$S_i = \frac{\Delta P_i}{\Delta x_i} = \left(\mu \cdot D_{ij} + \frac{1}{2} \cdot F_{ij} \cdot \rho \cdot |u|\right) \cdot u_i \quad (1)$$

with $D_{ij} = \begin{bmatrix} D_x & 0 & 0 \\ 0 & D_y & 0 \\ 0 & 0 & D_z \end{bmatrix}$

and $F_{ij} = \begin{bmatrix} F_x & 0 & 0 \\ 0 & F_y & 0 \\ 0 & 0 & F_z \end{bmatrix}$

Here μ is the air dynamic viscosity (in pa s), ρ is the air density (in kg m^{-3}), $|u|$ is the velocity magnitude and u_i the velocity in the i direction (both in m s^{-1}), D_{ij} and F_{ij} are the viscous resistance coefficients (in m^{-1}) and the inertial resistance coefficients (in m^{-2}), respectively. The linear term, called the viscous term, has been introduced by Darcy (1857) and corresponds to laminar flow (low Reynolds number). It is characterized by the permeability of the porous medium. The quadratic term, called
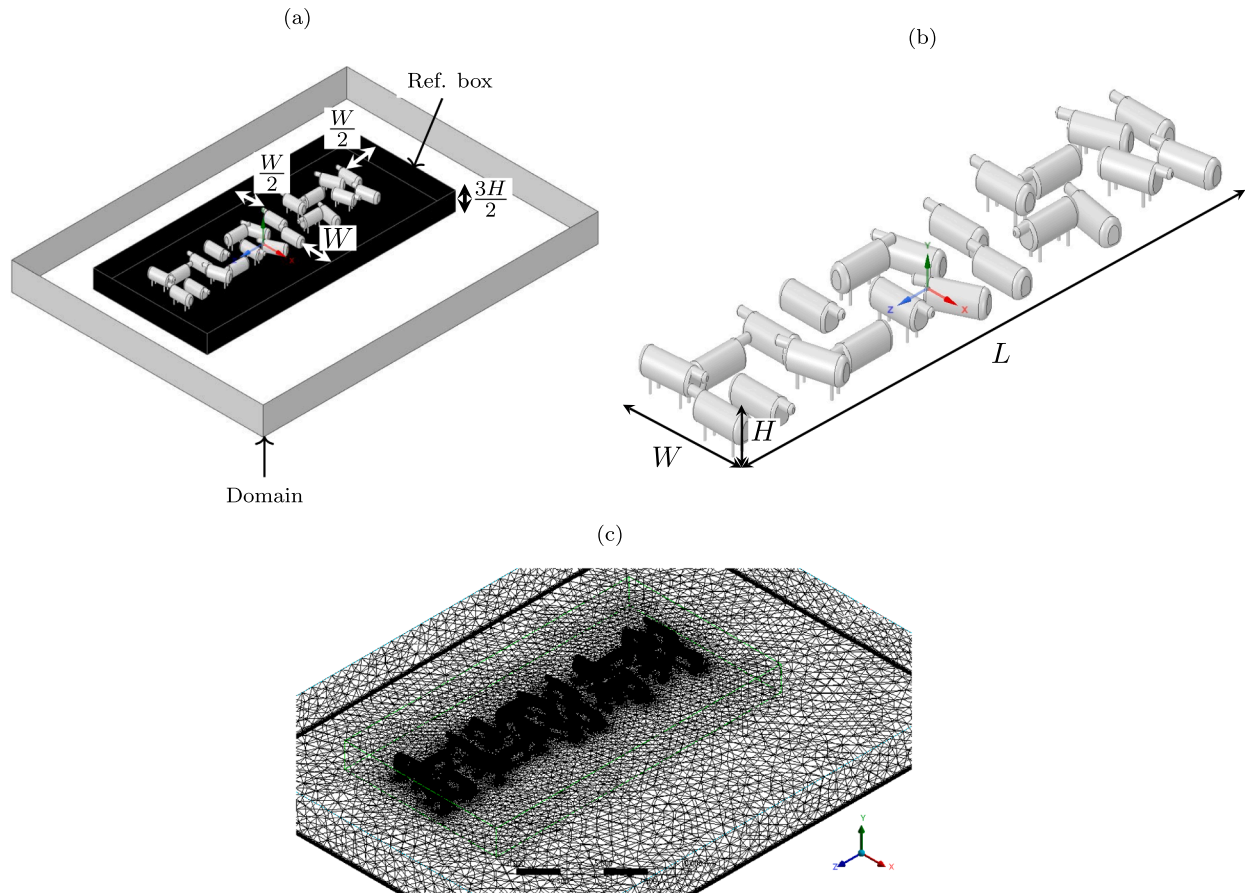

Fig. 1. (a) Domain and refinement box dimensions, (b) Animal occupied zone with 22 lying and standing cows aligned in 2 rows, (c) Corresponding mesh, cell size 0.8 m for the domain and 0.4 m for the mesh refinement sub-domain.

the inertial term, has been added later on by Forchheimer (1901) and describes the effects of turbulence (high Reynolds number). In this study the local Reynolds number cover the range from $1.6 \cdot 10^4$ until $4.36 \cdot 10^5$ which corresponds to fully turbulent flow.

The viscous resistance D and the inertial resistance F characterize the pressure drop. They are the input values for the porous modeling. For homogeneous porous media $Dx = Dy = Dz$ and $Fx = Fy = Fz$. However due to the heterogeneous shape of the AOZ, Fig. 2, in our case the co-efficients for each main direction are expected to diverge from each other, i.e. $Dx \neq Dy \neq Dz$ and $Fx \neq Fy \neq Fz$. Thus, for each main direction we determine the viscous and inertial resistance using the regression approach described by Simonsen et al. (2006).

For different inlet velocities (0.1; 0.5; 1.2; 2 and 3 m s^{-1}) the pressure drop per meter of the AOZ has been determined as a difference of the mean pressure of planes (dimensions: $L \cdot H$ in the x direction, $W \cdot H$ in the z direction and $L \cdot W$ in the y direction) at the front and the back of the AOZ in the flow direction, see Fig. 2. For each main direction, the function $\Delta P_i \cdot \Delta x_i^{-1} = f(u_i)$ has been derived. From the regression, the coefficients F_i and D_i have been extracted and implemented in the PMM. The pro-cedure is sketched in Fig. 2. In order to enhance further the accuracy of the PMM an iterative approach has been used. With Ansys "Direct optimization" tool, each $\Delta P_i \cdot \Delta x_i^{-1}$ from the cows model (CM) was set as target value for the porous model. As input, the user has to provide a range of values for F_i and D_i, and the target $\Delta P_i \cdot \Delta x_i^{-1}$ that the PMM should have. Beginning from randomly chosen values of F_i and D_i, Ansys direct optimization, with an Ansys-inbuilt algorithm, looks iteratively for the candidate values of F_i and D_i that match the target pressure drop $\Delta P_i \cdot \Delta x_i^{-1}$. At the end, for each velocity the optimal F_i and D_i have been found.

2.2.1. Velocity profiles and air exchange rate evaluation

The velocity profiles downstream of the AOZ will be compared for both models. The three vertical red lines (of $1.5 \cdot H$ height each) for the velocity evaluation have a distance W between them, Fig. 3.

The air exchange rate (AER) of an AOZ was calculated using the equation Eq. 2.

$$AER = \frac{3600 \cdot \dot{V}}{V_{AER}} \tag{2}$$

Here AER is the air exchange rate of the volume V_{AER} (in h^{-1}), $\dot{V}$ is the sum of volume flow entering in V_{AER} (in m^3 s^{-1}) and V_{AER} the considered volume for AER evaluation (in m^3). In our study the considered volume $V_{AER} = W \cdot L \cdot 2H$ had twice the height of the animal occupied zone, taking thus into account the immediate air flow above and produced by the cows. The height should at least cover the height of the AOZ, but the modelling of the AOZ affects also the flow right above the AOZ. The

larger the height the less effect of the AOZ parametrization on the local volume flow can be expected. Hence, the selected height of $2H$ is considered a suitable compromise.

2.3. Heat transfer modeling

In order to model the heat transfer through the porous medium, the following term has been added to the conservation equation (ANSYS, 2019):

$$A_{fs} \cdot h_{fs} \cdot (T_s - T_f) \text{ for fluid zone} \tag{3}$$

$$A_{fs} \cdot h_{fs} \cdot (T_f - T_s) \text{ for solid zone} \tag{4}$$

Here A_{fs} is the interfacial area density, i.e. ratio between the solid/fluid interface area and the fluid volume (in m^{-1}), h_{fs} is the interstitial heat transfer coefficient between the fluid/solid interface (in W m^{-2} K^{-1}), T_s is the solid temperature which is in our case the cow surface temperature (in K) and T_f is the fluid temperature which is our case the inlet air temperature (in K). For our case the "non equilibrium thermal model" has been chosen. This means that in the porous medium the fluid part and the solid part have their own temperature separately. In Ansys, for the given porosity, a "virtual" solid zone is created inside the porous medium and acts solely as a heat source for the heat transfer (no pressure drop added) between the fluid and the porous media. The heat transfer is characterized by the heat transfer coefficient h_{fs}. It corresponds to the same heat transfer coefficient between the fully modeled cows and the fluid h_{cows}. For model simplification purpose, this work focuses on convective heat transfer only and the other types of heat transfer such as radiations (the one emitted by the cows into the surroundings and the other coming from sun) and conductions (through the barn's ground) are neglected. Our work follows the method described by Jeremy (2017) to find out the convective heat transfer coefficient from a porous me-dium. As pictured in Fig. 4, the AOZ is placed in a closed domain. This configuration forces the flow in one direction and thus simplifies the evaluation of the energy balance. As an analogy of the heat transfer of a flow inside a pipe with a constant wall temperature, the total convective heat transfer can be considered as:

$$Q_{conv} = \dot{m} \cdot C_p \cdot (T_{in} - T_{out}) \tag{5}$$

$$Q_{conv} = h_{cows} \cdot A_s \cdot \Delta T_{log} \tag{6}$$

$$\Delta T_{log} = \frac{T_{out} - T_{in}}{ln \frac{T_{cow} - T_{out}}{T_{cow} - Tin}} \tag{7}$$

Here Q_{conv} is the convective heat transfer (in W), $\dot{m}$ is the mass flow rate (in kg s^{-1}), C_p is the cow surface specific heat capacity (in J kg^{-1} K^{-1}),
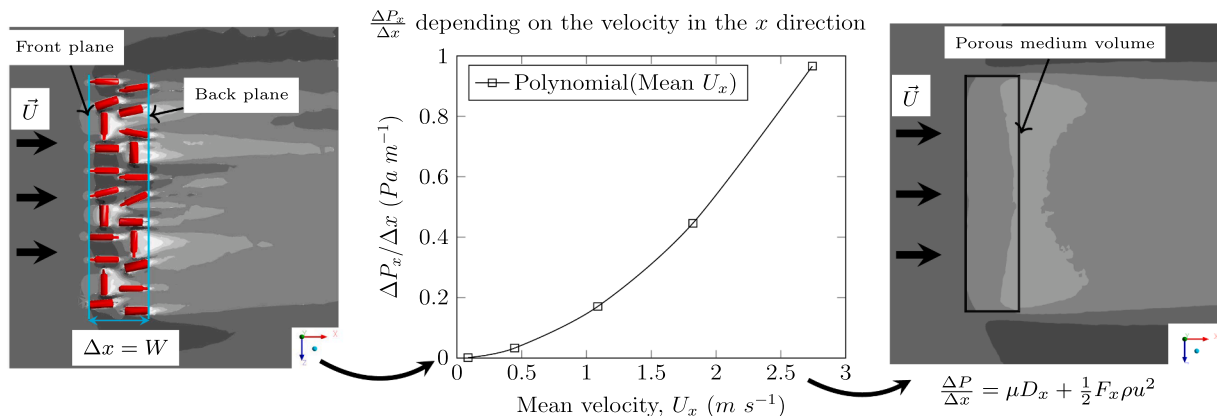

Fig. 2. Description of finding and implementing the viscous and inertial coefficients from the cows model pressure drop profile in the x-direction, the horizontal plane for the velocity contour is at the height of $H/2$.
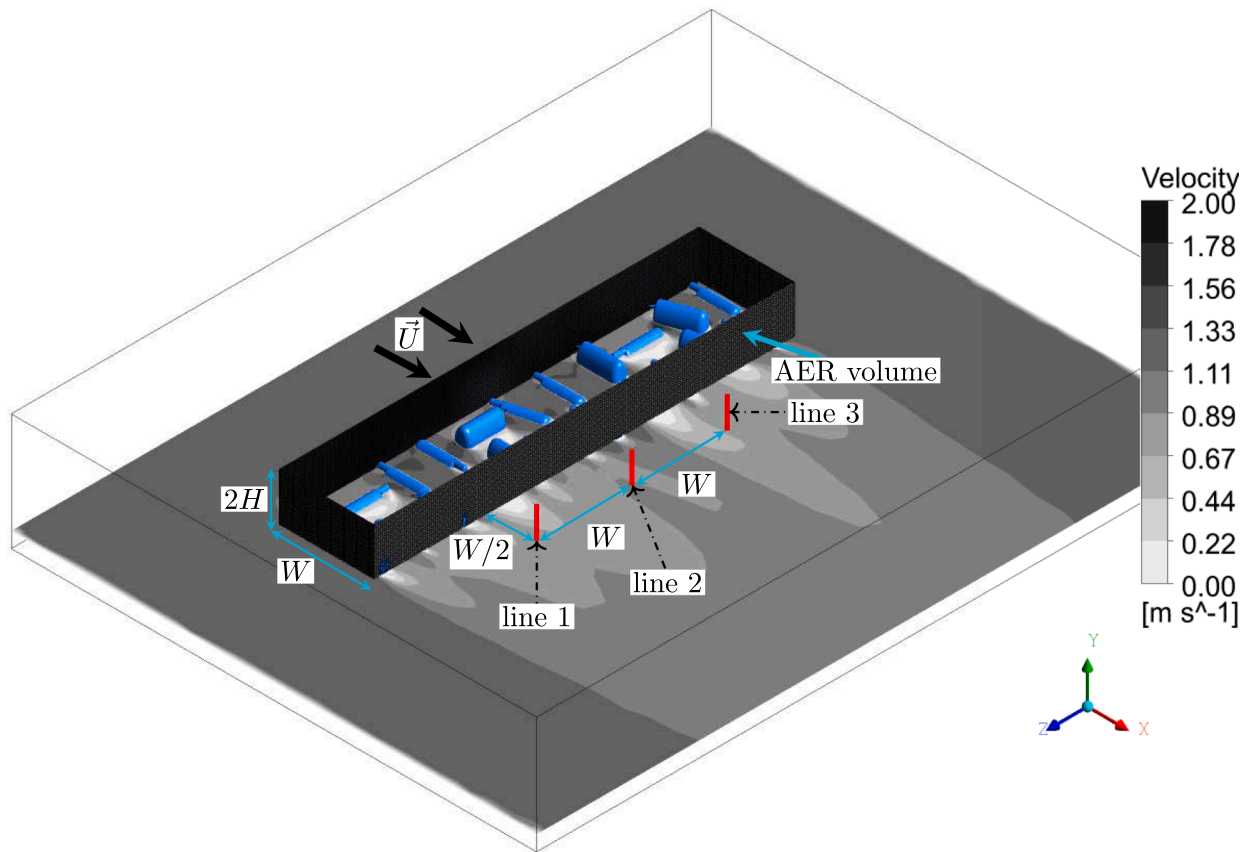
Fig. 3. Lines for velocity profiles and air exchange rate volume evaluation, the horizontal plane for the velocity contour is at the height of $H/2$.

Fig. 4. Configuration for heat transfer evaluation in close domain.

T_{in} and T_{out} are the inlet and outlet fluid temperature respectively (in K), h_{cows} is the heat transfer coefficient between cows and air (in W m^{-2} K^{-1}), A_s is the interface area between cows and air (in m^2), ΔT_{log} is calculated from T_{in} and T_{out} (in K). For the 3D cow modeled AOZ, the thermal cows' properties have been extracted from the work of Drewry et al. (2018). We have chosen 0.52 W m^{-1} K^{-1} for the cow thermal conductivity, 3472 J kg^{-1} K^{-1} for the cow specific heat capacity for a 3 mm conductive shell, which has been added on the cow surface temperature as a way to model the cow hair coat (Drewry et al., 2018; Wang et al., 2018). And a constant temperature of 38 °C (Mader et al., 2005) for the cow surface temperature has been fixed.

2.4. Convection type evaluation

Keeping the temperature gradient between the incoming air and the cow's surface ($\Delta T = T_{air} - T_{cows} = 20$ K) as constant, the requirement for the Boussinesq approximation for natural convection was valid:

$$\beta \cdot (T - T_O) \gg 1 \qquad (8)$$

where $\beta = T_m^{-1}$ (in K^{-1}) is the isobaric thermal expansion coefficient, with $T_m = 0.5 \cdot (T_{air} + T_{cows})$ (Marek and Nitsche, 2015) and T_O (in K) is the operating temperature, in our case T_{air}. The Boussinesq approximation is useful to obtain faster convergence since it models the natural

convection in steady calculation without the need to switch to transient calculation (ANSYS, 2019).

The Richardson number Ri, which is the ratio of the buoyancy forces and the kinetic forces, was used to distinct the 3 types of convection (Marek and Nitsche, 2015):

$$Ri = \frac{Gr}{Re^2} \qquad (9)$$

where Gr is the Grashof number and Re is the Reynolds number (both without dimension). As summarized in Table 2, when $Ri \gg 1$, the buoyancy forces represented by the Grashof number (Gr) prevail over the kinetic forces represented by the Reynolds number. When $Ri \approx 1$, the buoyancy forces are on par with the kinetic forces. And for $Ri \gg 1$, the

Table 2
Type of convective heat transfer and Ri values.

Type of convection	Ri values	
	In general	In our case
Forced	$\ll 1$	<0.2
Mixed	≈ 1	>0.2 and <5
Natural	$\gg 1$	>5

kinetic forces are dominant. The range 0.2–5 (corresponding to the velocities 2.6 m s^{-1} for $Ri = 0.2$ and 0.53 m s^{-1} for $Ri = 5$) for the mixed convection is extracted from (Marek and Nitsche, 2015) as practical values. One can obtain more precised value following the recommendation of Sparrow et al. (1959). However, since such a study would be out of the scope of the present manuscript, we choose to stick with the general boundary Ri values 0.2 and 5 for the different types of heat transfer convection. For more details the convection types, we advise both references cited above.

The simulation has been conducted in a large domain, allowing the observation of free type of convection, see Fig. 5 where the boundary conditions and the dimensions of the domain are detailed. The inlet velocity respects the atmospheric boundary layer profile through the equation (Blocken et al., 2007):

$$U_y = U_{ref} \cdot \left(\frac{y}{y_{ref}} \right)^{\alpha} \tag{10}$$

Here U_y is the inlet velocity profile (in m s^{-1}), U_{ref} is the chosen velocity (in m s^{-1}) at the height y_{ref} (in m) and α is a power coefficient (without dimension). The value of $\alpha = 0.16$ has been extracted from our wind tunnel measurements and corresponds to a moderately rough terrain.

One important note is the computing time. On 15 CPUs, for the CM the simulation took 75 min to run and for the PMM, it took only 6 min. Almost 90 % of the computing has been spared with the PMM.

2.5. On farm validation setup

The method described in this manuscript has been used for the numerical validation against on farm measurements. As a proof that replacing the AOZs by their corresponding porous mediums actually leads to a velocity distribution that matches the reality. The ATB-barn in Dummerstorf is composed of different AOZs (14, 18, 22, 28, 30, 42 and 44 standing and lying cows) leading to an overall number of 370 cows. A numerical simulation with such a large number of bodies would not be realistic in a matter of time and computational resources. The modeled barn, the porous volumes inside and its surroundings (buildings and trees) can be observed in Fig. 6. For this validation case, the air is incoming at 7°C with a velocity of 0.1578 m s^{-1} at 3 meters height. The vertical component of the velocity has been measured at different points at 3 meters height inside the barn by the WindMaster 3D Ultrasonic Anemometer, details in Fig. 7. Accordingly, in the numerical simulation vertical velocity at each of those points has been evaluated and compared with the on-farm measurements.

3. Results and discussion

3.1. Pressure drop modeling

In the left part of Table 3 the initial resistance values of F_i and D_i are summarized. Using those original values directly in the PMM does not produce a satisfactory result as shown in Fig. 9(a). The relative errors represented by the curves x_dir and z_dir are around 50%. In order to avoid this discrepancy, Ansys Fluent propose an alternative. The assumption is that the porous medium is an 100% open fluid volume and that the corresponding 3D object is the (100 x porosity)% open to the flow. Consequently, the pressure drop coefficients have to be adapted as followed $D_i \cdot porosity^{-2}$ for the viscous resistance and $F_i \cdot porosity^{-1}$ for the inertial resistance. The modified coefficients have been deduced and presented in the right part of Table 3. However, that is still not satisfactory enough as can be noticed in Fig. 9(a), the errors represented by the curves x_dir mod and z_dir mod are around 40%. For this reason we had to resort to the iterative process, explained in the method Section 2.2, in order to reach a pressure drop of a PMM that is as near as possible to the CM.

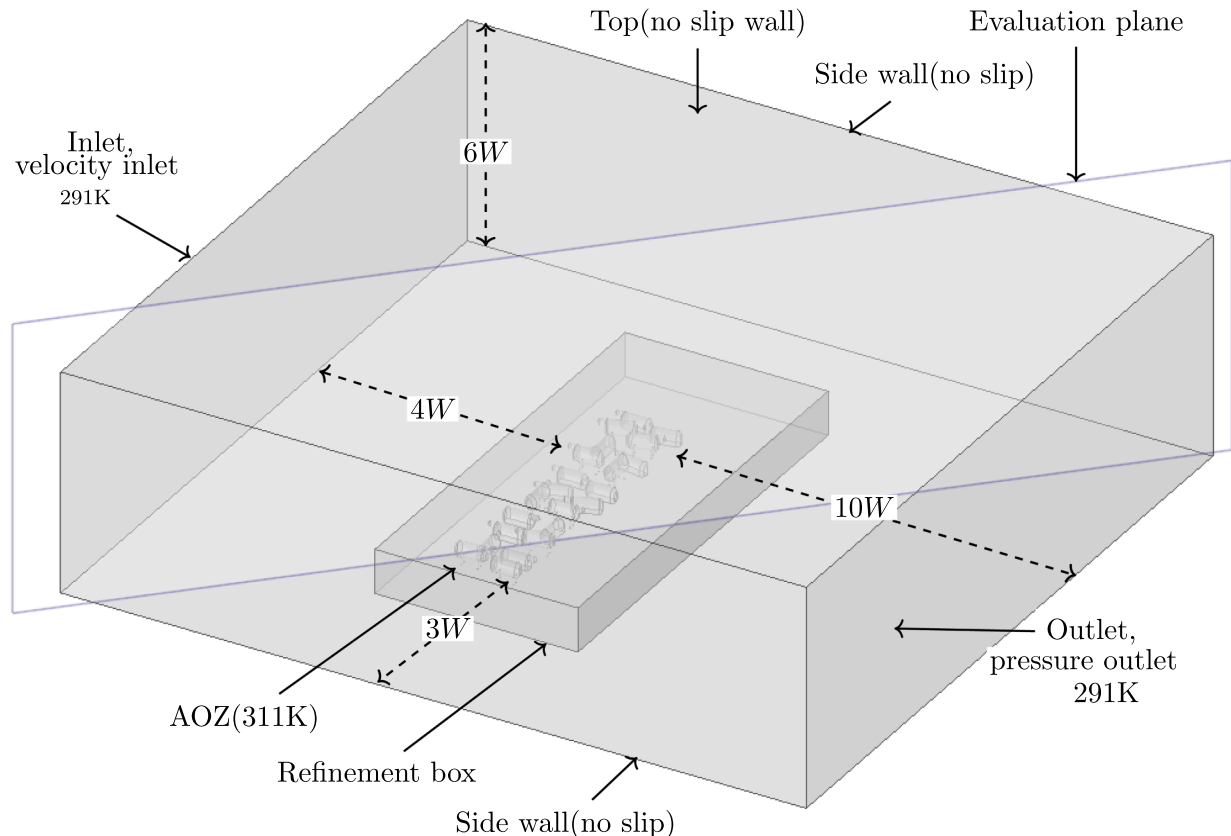A velocity dependency has been observed and functions $F_i(u)$ and

Fig. 5. Boundary conditions and dimensions of the domain for convective flow.
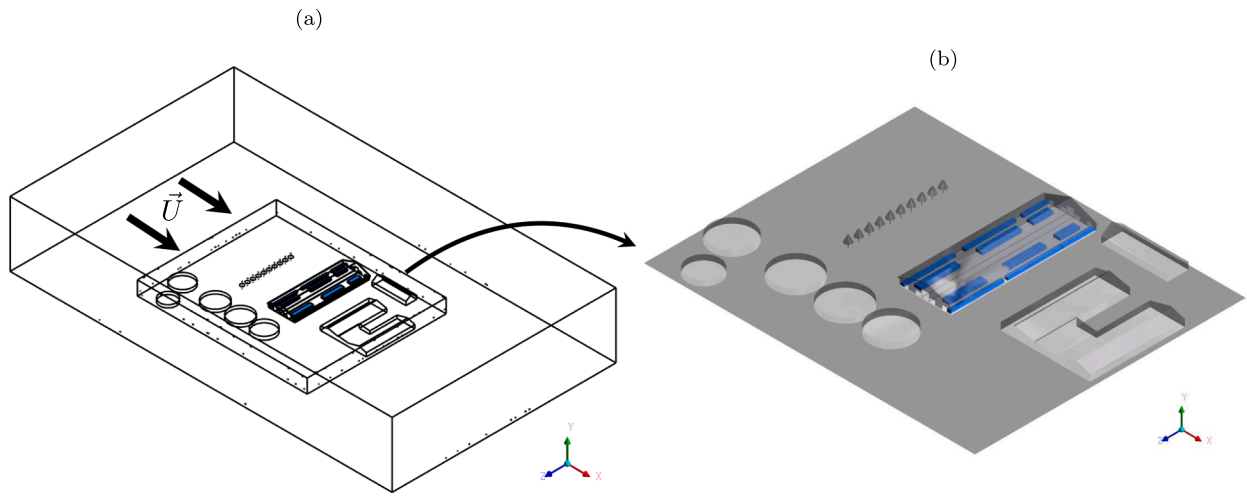
Fig. 6. Overview of animal barn. (a) Whole computation domain, (b) animal barn and its surroundings.
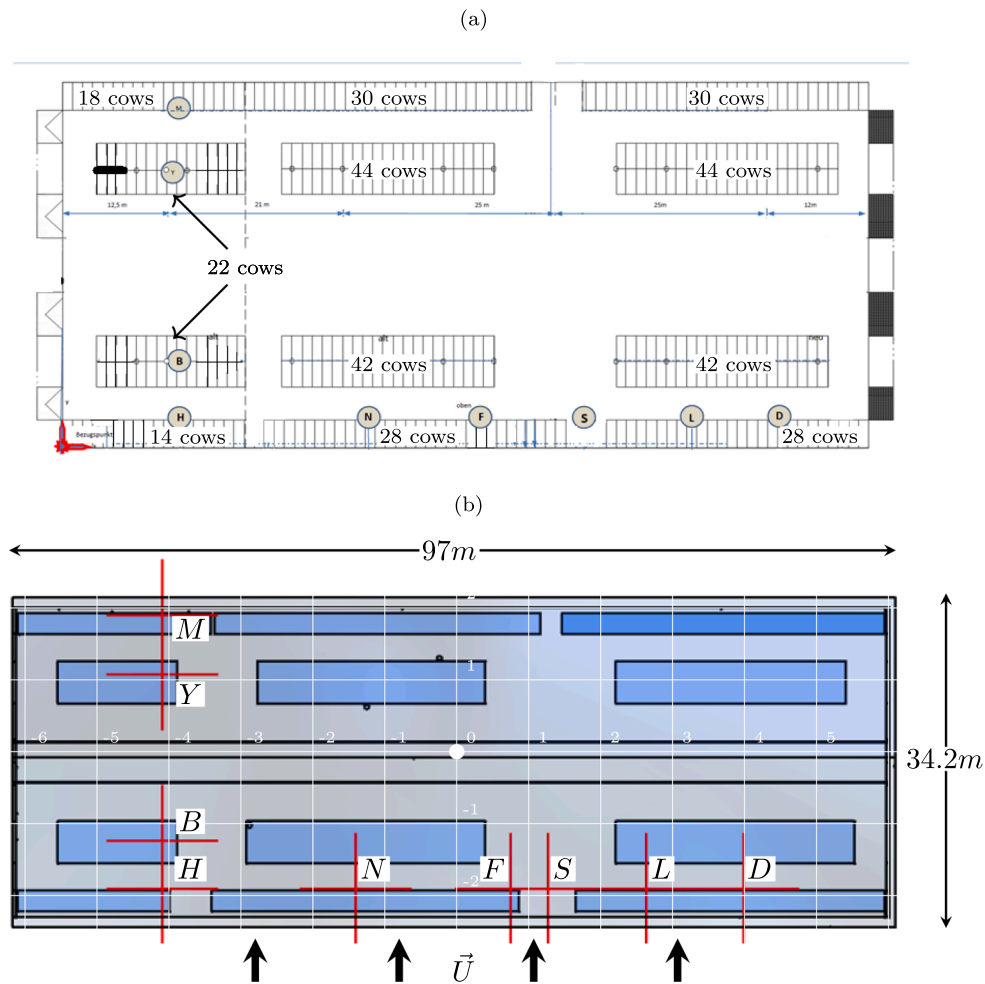

Fig. 7. (a) Dummerstorf barn AOZs plan, (b) Corresponding porous mediums in the numerical simulation.

$D_i(u)$ were derived, see Fig. 8 for the case of flow in the z direction. The functions describing the resistance parameter can be linear, power or logarithmic depending on the considered AOZ and the flow direction. In our case, the functions with the least regression error were a logarithmic equation for the viscous resistance coefficient and a power law equation inertial resistance coefficient. After implementing those functions in the porous model, the obtained pressure drop error between the CM and the

PMM ($= |\Delta P_{CM} - \Delta P_{PMM}| \cdot \Delta P_{CM}^{-1} \cdot 100$, with ΔP_{CM} being the pressure drop in the cow model, and ΔP_{PMM} being the pressure drop in the porous medium model) for the flows in x and z directions, as shown in Fig. 9(b), has been reduced to below 5% with an average of 1.5% for the considered velocity values. Yin et al. (2016) obtained the same range of precision when modelling slatted floors with porous medium. Hence, the results confirm a high accuracy when using a porous medium approach

Table 3
Original and modified values of D_i and F_i coefficients.

Inflow direction	Original constants			Modified constants		
	To the front (U_x)	To the side (U_z)	From above (U_y)	To the front (U_x)	To the side (U_z)	From above (U_y)
D [m^{-2}]	1536.83	1581.54	20671.73	1905.29	1960.71	25627.84
F [m^{-1}]	0.19	0.11	0.14	0.30	0.17	0.21

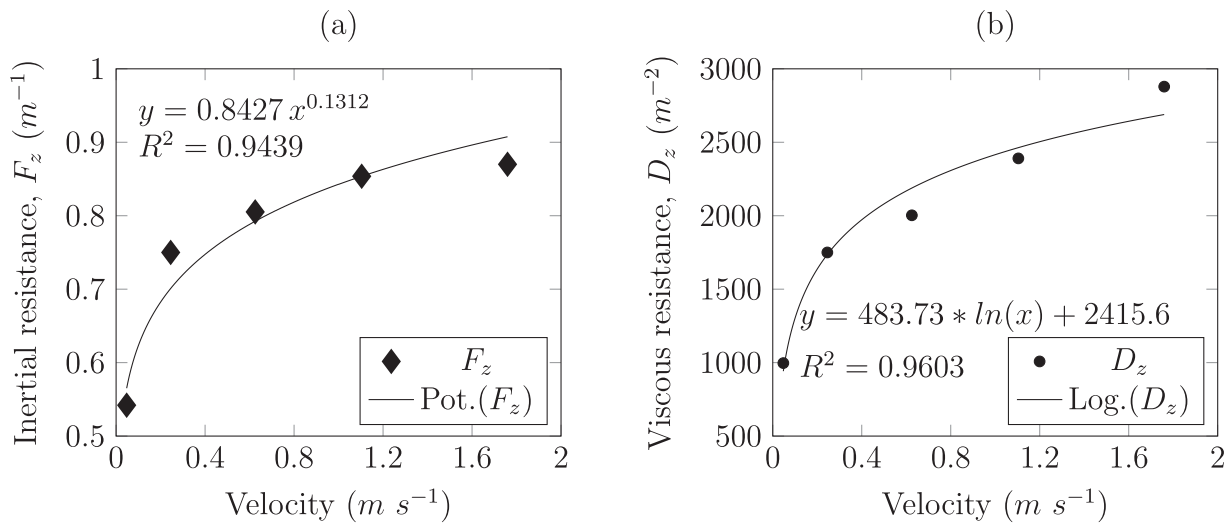**Fig. 8.** F_z (a) and D_z (b) values coefficient depending on the velocity.
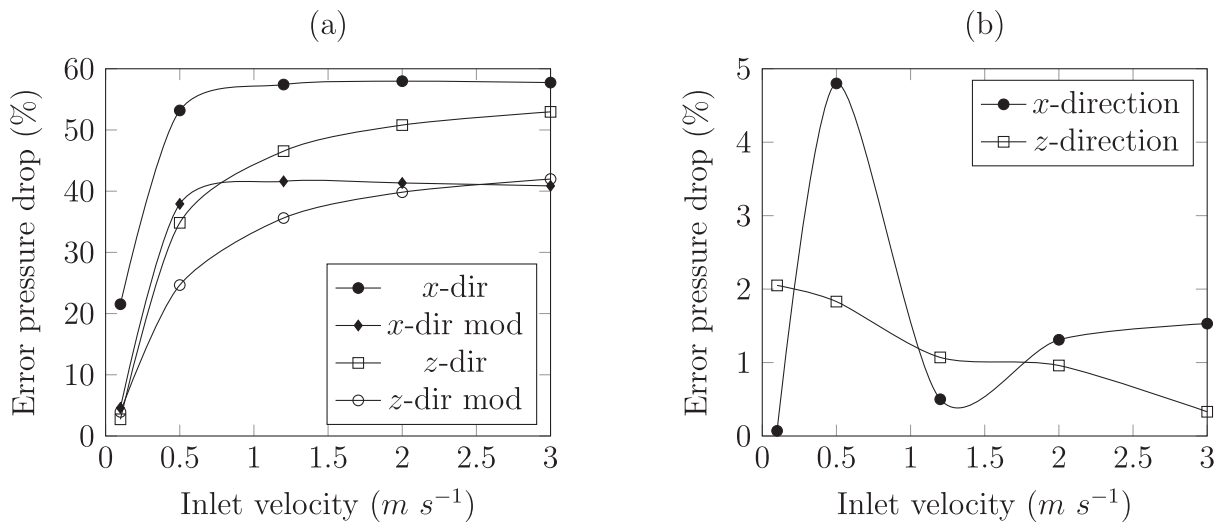

Fig. 9. Error pressure drop between the cows and porous model for main flow incoming to front(x) and side(z), (a) from (original and modified) constants coefficients, (b) from velocity dependent coefficients.

to represent the AOZ of cows. For the y direction, the coefficients F_y and D_y have been kept as constant, because of the small improvements in this direction. This may be due to the small thickness of the AOZ in the y direction compared to the other directions, $\Delta y = 1.6$ m, while $\Delta x = 4.9$ m and $\Delta z = 10.8$ m.

The vertical velocity profiles have been compared between both models at a distance W away from the AOZ, cf Fig. 3 from evaluation methods part. The comparison of the velocity profiles in Fig. 10(a) shows that at the side lines (line 1 and 3), the profiles for the PMM are almost exactly the same. For the CM the velocity profiles are distant from each other, especially for the middle line. It has to be noted that the

PMM, even with velocity adaptive coefficients, is unable to completely reproduce the complexity of the flow resulting from the CM. This limitation should be taken into account when using the PMM.

Another practical relevant entity is the air exchange rate, which directly related to the volume flow rate. Because it is directly related to the animal welfare in the AOZ (Fiedler et al., 2012). The deviation of the AER from the PMM compared to the CM is shown in Fig. 10(b). It can be observed that the discrepancy between the AERs calculated by the PMM and the CM is negligible. The relative error ($= (AER_{cows} - AER_{porous}) \cdot AER_{cows}^{-1} \cdot 100$) has an average value below 2%.
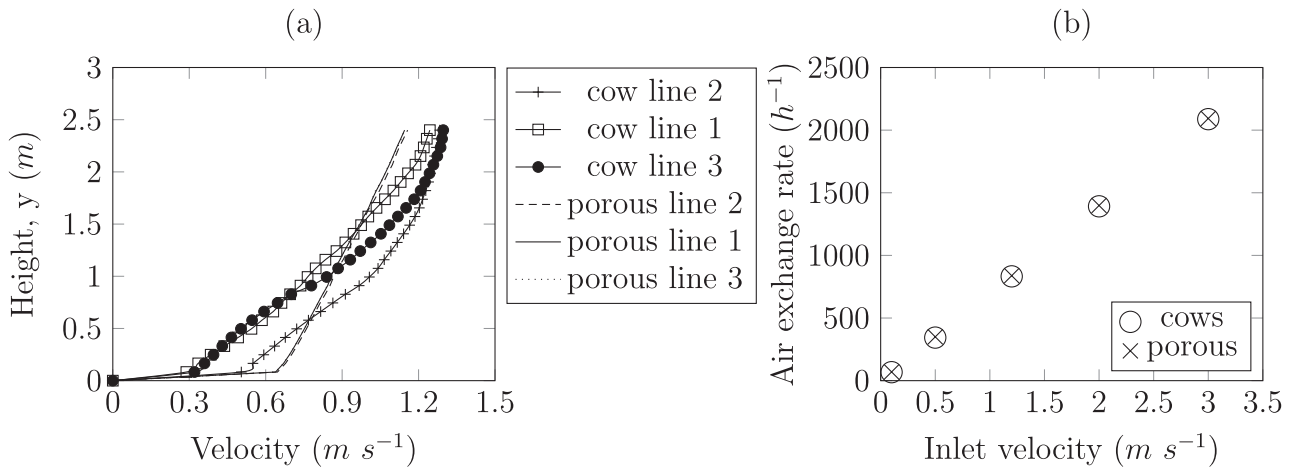
Fig. 10. (a) Vertical Velocity comparison between cows and porous model, (b) AER of AOZ comparison between the porous and cows model for the case with main flow in *x*-direction.

3.2. Heat transfer modeling

The heat transfer coefficient h_{cows} calculated from the simulated CM for different constant velocity (or mass flow rate), is shown in Fig. 11(a). The heat transfer coefficient is known to be a function of the Nusselt number, which depends on the values of the Reynolds, Prandtl and Rayleigh numbers. From those well-known relations, the heat transfer coefficient is expected to increase with the velocity, where its value in general can vary from about 0.5 to 100 000 W m^{-2} K^{-1}. As reported earlier (e.g., by Wang et al. (2018)), the velocity-dependency of the convective heat transfer coefficient is clearly visible in the context of airflow around cows. In our study with multiple cows, the h_{cows} values are within the range of the values of 4.816 W m^{-2} K^{-1} reported by Wang et al. (2018) for one standing cow. The dependence of the heat transfer coefficient has been found to be well described by a linear function in our range of application, while in the work of Jeremy (2017) it was an exponential function. Implementing the obtained h_{cows} as a function of the velocity as parameter h_{fs} in the PMM, we obtain the error curve shown in Fig. 11(b). The comparison of the convective heat transfer between the CM and the PMM shows in general smaller relative errors ($|Q_{convcow} - Q_{convporous}| \cdot Q_{convcow}^{-1} \cdot 100$) for lower velocities, except for very low velocity. The results show an error below 6% with an average of 2.9%.

3.3. Velocity and temperature distribution

Fig. 12 presents a comparison of the temperature and velocity distributions between the PMM and the CM for the cases of natural convection ($Ri \gg 1$), where the heat transfer considerably affects the emerging flow pattern. Since the buoyancy forces (Gr) prevail over with kinetic forces (Re), the buoyancy-driven flow can be easier seen. The inlet velocity angle is of 45 degree. Implementing the heat transfer coefficient as a velocity adaptive function gives a temperature and velocity distribution of the PMM case in accordance with the CM case. The maximum temperature and velocity have been found to be in the same order of magnitude in both models. Furthermore, the positions of the maximum temperature and velocity are similar. The main deviations have been found above the AOZ where the temperature and velocity distributions are smoother in the PMM. The average air flow in the vicinity of the AOZ was, however, well reproduced by the PMM model.

In Table 4 three porous models are compared with the CM: First, the porous model with the anisotropic velocity dependent pressure drop coefficients ($Dx(u) \neq Dy(u) \neq Dz(u)$ and $Fx(u) \neq Fy(u) \neq Fz(u)$) and velocity dependent heat transfer coefficient ($h = f(u)$), Aniso f(u). Then, the PMM characterised by anisotropic pressure drop with constant coefficients ($Dx \neq Dy \neq Dz$ and $Fx \neq Fy \neq Fz$, but all original constants values from Table 2) and constant heat transfer coefficient ($h = $ constant), Aniso const. And finally, the PMM characterised by isotropic
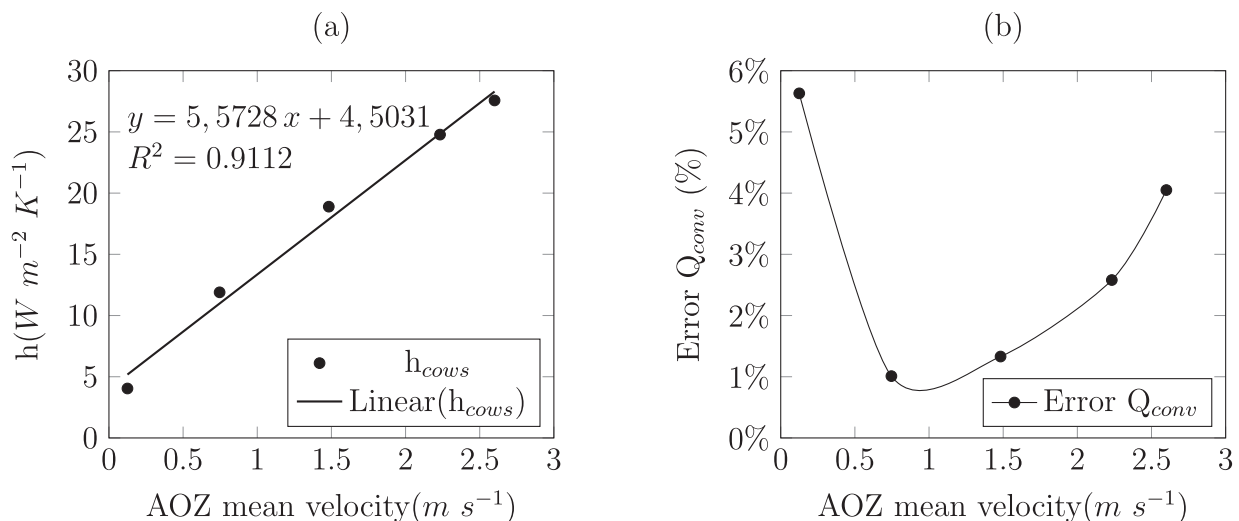

Fig. 11. (a) Heat transfer coefficient from cows model; (b) Convective heat transfer error between cows and porous model.
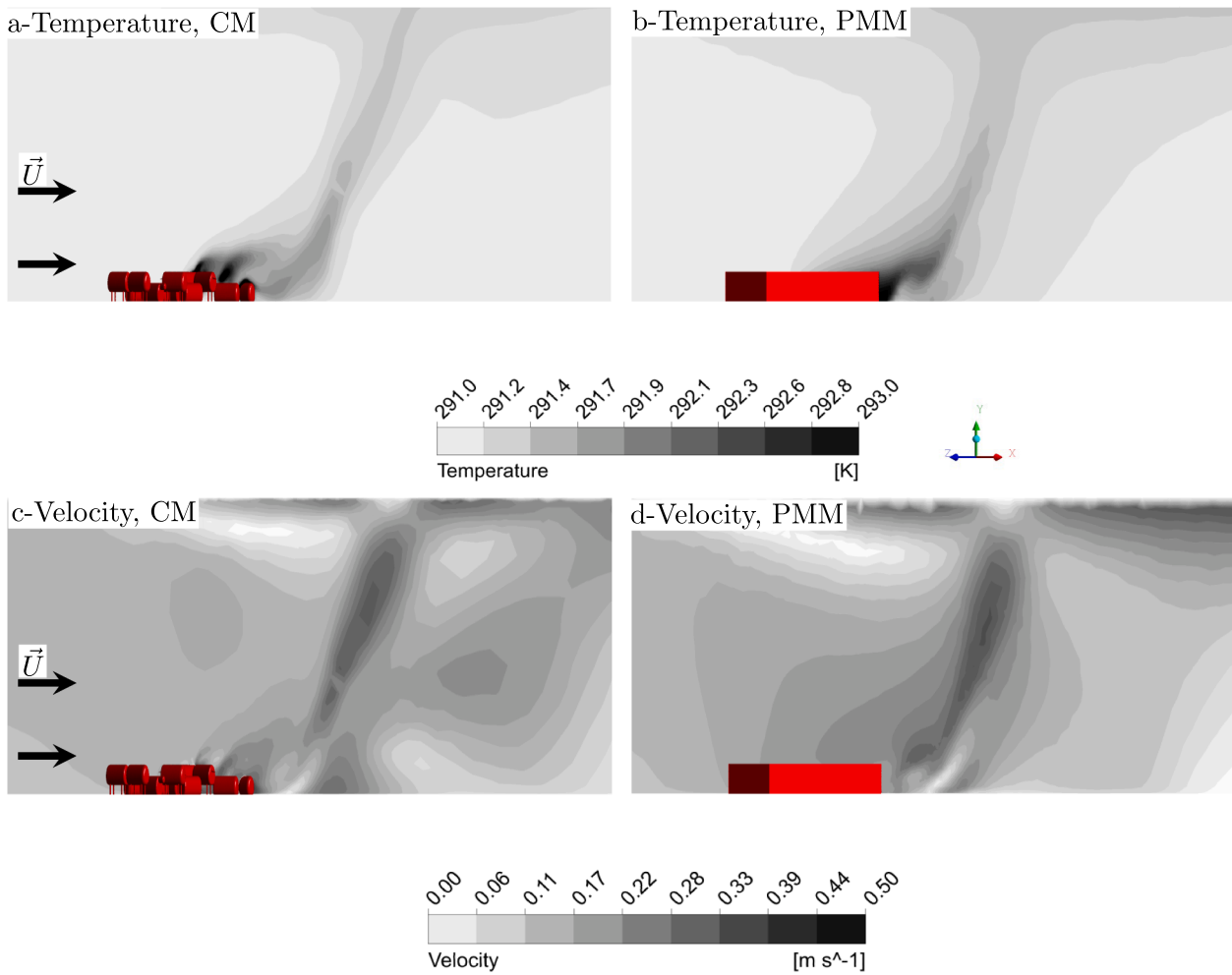
Fig. 12. Evaluation plane in 45 degree direction inside the domain, temperature (a, b) and velocity (c, d) distribution in the case of natural convection, (a, c) cows model, (b, d) porous medium model, for 45 degree inlet velocity.

Table 4
AER comparison between the CM, our anisotropic PMM with velocitiy-dependent coefficients and an anisotropic PMM with constant coefficients as well as an isotropic PMM for the different convection types with 45 degree inlet velocity.

Type of convection	AER CM (h^{-1})	Aniso f(u) (h^{-1})	rel. Error (%)	Aniso const (h^{-1})	rel. Error (%)	Iso const (h^{-1})	rel. Error (%)
Natural ($Ri > 5$)	137.53	151.12	9.88	161.46	17.40	160.95	17.03
Mixed ($Ri = 1$)	648.82	668.46	3.03	719.44	10.88	715.64	10.30
Forced ($Ri < 5$)	1868.51	1923.05	2.92	2070.12	10.79	2059.47	10.22

pressure drop with constant equal coefficients (*Dx* and *Fx* are constants from Table 2, $Dy = Dz = Dx$ and $Fy = Fz = Fx$) and constant heat transfer coefficient ($h = $ constant), Iso const. The difference can be quantitatively observed through the AER for each convection type, evaluated and summarized in Table 4. The relative AER error $\left(= |AER_{CM} - AER_{Aniso\_f(u)}| \cdot AER_{CM}^{-1} \cdot 100 \right)$ is between 2.9% and 10% for the anisotropic velocity dependent PMM. While, for the other two PMMs relative AER errors are between 10% and 18%. This shows the gain in accuracy achieved by the developed porous model.

3.4. Validation with on-farm measurements

Fig. 13 summarizes the simulated vertical velocity at the evaluation points against the measurements. First of all, it can be noticed that the measured and simulated velocities are in the same range and, except for point B, in the same direction. On one hand the biggest discrepancy concern the point B, M and S. Due the fluctuating unsteady nature of the real flow, and the range of the velocity magnitude, such discrepancies can be expected. On the other hand, on the points D, F, H, L, N and Y the values are matching each other pretty well. This proves that the use of porous media to replace actual 3D cows geometries in the current setting is actually a solid approach.

4. Conclusion

Our study has shown that in turbulent regimes it is advisable to consider the AOZ as anisotropic when implementing a porous model. We could identify logarithmic, power law and linear functions to describe
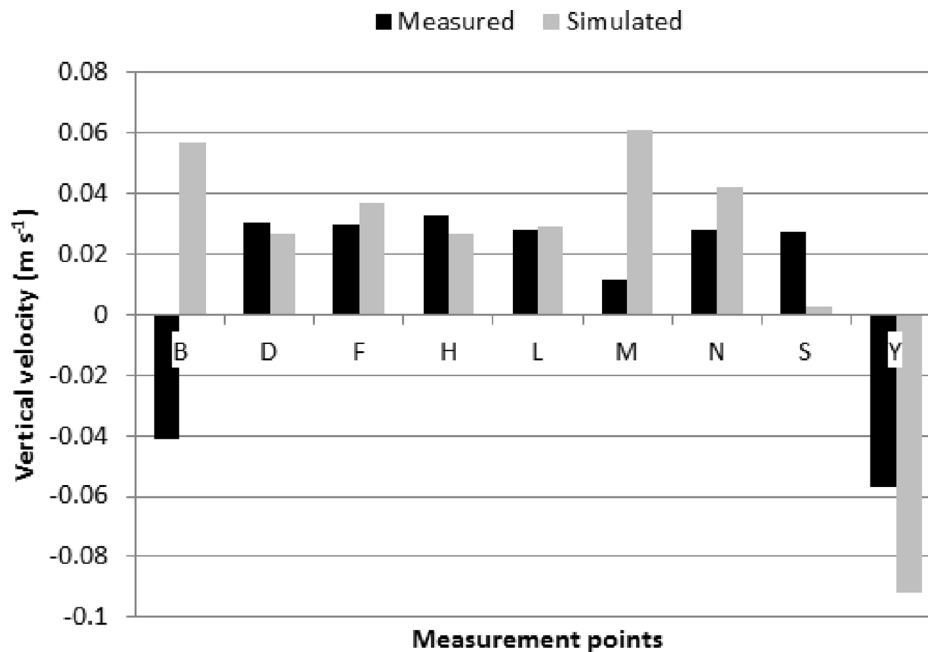
Fig. 13. Comparison between measured and simulated vertical velocities at the measurement points.

the relationships of viscous resistance, inertial resistance or heat transfer coefficient on the velocity. We have shown that this approach allows high accuracy of the PMM in terms of pressure drop, heat transfer and AER confirming the hypothesis nominated in the introduction. However, care must be taken when using the PMM especially in the evaluation of the local velocity and temperature distribution in the after flow, since the PMM can not reproduce the flow disturbances produced by the CM 3D geometries. Consequently, instead of a local evaluation, we advice a global or volumetric evaluation of the entities when using the PMM. The PMM showed a reliable prediction of the AER (which is a volumetric evaluation) with a difference of 3–10% compared with the results from CM. This was further demonstrated by the validation of our numerical simulation with PPM against on farm measurements. At four of nine measurement points the simulated velocity deviated from the measurements by on average of 14%. The other points, except for one, showed the right trend with deviations between 50% and 442%, while the absolute value of the air speed was in all cases below 0.1 m/s. The remaining point showed the wrong direction, but the deviation in the air speed was close to the measurement accuracy. We also showed that the accuracy of the method is not dependent of the arrangement and number of the animals of the CM, as long as the according functions and characteristics are implemented in the corresponding PMM.

Sparing up to 90% of computing time compared with a model with resolved cow geometry, while keeping a good level of accuracy in terms of flow resistance and heat transfer opens the door to new possibilities, like simulations of buildings with a large number of animals. Our results indicate that it is acceptable to use PMM in the proposed setting instead of hundreds of modeled cows for future studies while focusing on the evaluation of the flow and temperature patterns inside and around dairy barns. This will save a fairly amount of computing power and time and enable more comprehensive parametric studies with large numbers of variations to be done in a short period of time.

Declaration of Competing Interest

The authors declare that they have no known competing financial interests or personal relationships that could have appeared to influence the work reported in this paper.

References

Ahmadi, S.F., Sefidvash, F., 2018. Study of pressure drop in fixed bed reactor using a computational fluid dynamics (cfd) code. ChemEngineering 2.

ANSYS, I., 2019. Ansys User Guide. URL http://www.ansys.com.

Bjerg, B., 2011. CFD Analyses of Methods to Improve Air Quality and Efficiency of Air Cleaning in Pig Production. InTech, pp. 639–654 (Chapter 24).

Blocken, B., Stathopoulos, T., Carmeliet, J., 01 2007. Cfd simulation of the atmospheric boundary layer: wall function problems. Atmos. Environ. 41, 238–252.

Bustos-Vanegas, J.D., Hempel, S., Janke, D., Doumbia, M., Streng, J., Amon, T., 2019. Numerical simulation of airflow in animal occupied zones in a dairy cattle building. Biosyst. Eng. 186, 100–105.

Darcy, H., 1857. Recherches expérimentales relatives au mouvement de l'eau dans les tuyaux. No. v. 1 in Recherches expérimentales relatives au mouvement de l'eau dans les tuyaux. Impr. Impériale. https://books.google.fr/books?id=s88WAAAAQAAJ.

Defraeye, T., Herremans, E., Verboven, P., Carmeliet, J., Nicolaï, B., 2012. Convective heat and mass exchange at surfaces of horticultural products: A microscale cfd modelling approach. Agric. For. Meteorol. 162–163, 71–84.

Doumbia, M., Hempel, S., Janke, D., Amon, T., 2019. Prediction of the local air exchange rate in animal occupied zones of a naturally ventilated barn. In: XXXVIII CIOSTA & CIGR V. XXXVIII CIOSTA & CIGR V International Conference, Rhodes Island, Greece, pp. 29–34.

Drewry, J., Mondaca, M., Luck, B., Choi, C., 01 2018. A computational fluid dynamics model of biological heat and gas generation in a dairy holding area. Trans. ASABE 61, 449–460.

Fiedler, M., Hoffmann, G., Loebsin, C., Berg, W., von Bobrutzki, K., Ammon, C., Amon, T., 2012. Luftgeschwindigkeit und hitzebelastung im milchviehstall - auswirkungen auf das tierwohl. LANDTECHNIK 67 (6), 421–424. https://www.lan dtechnik-online.eu/landtechnik/article/view/2012-67-6-421-424.

Forchheimer, P., 1901. Wasserbewegung durch Boden, 45th ed., vol. 1782–1788. Zeitschrift des Vereins deutscher Ingenieure, Düsseldorf.

Gebremedhin, K., Wu, B., 2005. Simulation of flow field of a ventilated and occupied animal space with different inlet and outlet conditions. J. Therm. Biol. 30 (5), 343–353. https://eurekamag.com/research/004/318/004318685.php.

Jeremy, V., 2017. Modelling of convective heat transfer in porous media. Master's thesis, The University of Western Ontario, Scholarship@Western. URL https://ir.lib.uwo.ca /etd/4852.

Kiwan, A., Berg, W., Brunsch, R., Eren Ozcan, S., Müller, H.-J., Gläser, M., Fiedler, M., Ammon, C., Berckmans, D., 2012. Tracer gas technique, air velocity measurement and natural ventilation method for estimating ventilation rates through naturally ventilated barns. Agric. Eng. Int. CIGR J. 14, 22–36.

Lanfrit, M., 2005. Best practice guidelines for handling automotive external aerodynamics with fluent.

Mader, T.L., Davis, M.S., Kreikemeier, W.M., 2005. Case study: Tympanic temperature and behavior associated with moving feedlot cattle1,2. Profess. Anim. Sci. 21, 339–344.

Marek, R., Nitsche, K., 2015. Praxis der Wärmeübertragung Grundlagen - Anwendungen - Übungsaufgaben, fourth ed. Carl Hanser Verlag GmbH & Co, KG.

Mendes, L., Rocha, K.S., Azevedo, E., Ogink, N., Tinoco, I., Dooren, H.J., Mosquera, J., Osorio Saraz, A., 2014. Air motion patterns in a naturally ventilated dairy barn by means of a cfd model combined with the carbon dioxide mass balance method.

Mondaca, M., Choi, C., 2015. Assessment of dairy cow geometries in computational modeling. In: 2015 ASABE Annual International Meeting, 1–6.

Patursson, O., Swift, M., Tsukrov, I., Simonsen, K., Baldwin, K., Fredriksson, D., Celikkol, B., 2010. Development of a porous media model with application to flow through and around a net panel. Ocean Eng. 37, 314–324.

Rong, L., Elhadidi, B., Khalifa, H., Nielsen, P., 2010. Cfd modeling of airflow in a livestock building. In: Abstract Book: Clima 2010: 9–12 May, Antalya. Clima 2010: 10th Rehva World Congress, p. 457, null; Conference date: 09–05-2010 Through 12–05-2010.

Saha, C., Fiedler, A., Amon, T., Berg, W., Amon, B., Brunsch, R., 2014. Assessing effects of different opening combinations on airflow pattern and air exchange rate of a naturally ventilated dairy building - a cfd approach. In: International Conference of Agricultural Engineering, Zurich.

Simonsen, K., Tsukrov, I., Baldwin, K., Swift, M.R., Patursson, O.E., 2006. Modeling flow through and around a net panel using computational fluid dynamics. In: OCEANS 2006. pp. 1–5.

Sparrow, E., Eichhorn, R., Gregg, J., 1959. Combined forced and free convection in a boundary layer flow. Phys. Fluids 2 (3), 319–328.

Stamou, A., Katsiris, I., 2006. Verification of a cfd model for indoor airflow and heat transfer. Build. Environ. 41, 1171–1181.

The Danish Agricultural Advisory Center, 2001. Interdisciplinary report Housing Design for Cattle - Danish Recommendations. Third edition 2001. The Danish Agricultural Advisory Center, translated into English and issued in 2002, 122p.

Tiwary, A., Morvan, H., 2006. Modelling the size-dependent collection efficiency of hedgerows for ambient aerosols. J. Aerosol Sci. 37, 990–1015.

Wang, X., Zhang, G., Choi, C., 2018. Effect of airflow speed and direction on convective heat transfer of standing and reclining cows. Biosyst. Eng. 167, 87–98.

Yin, S., van 't Ooster, B., Ogink, N., Groot Koerkamp, P., 2016. Assessment of porous media instead of slatted floor for modelling the airflow and ammonia emission in the pit headspace. Comput. Electron. Agric. 123, 163–175.

Zhou, J.-Q., Wang, L., Cardenas, M., 2019. Universal relationship between viscous and inertial permeability of geologic porous media. Geophys. Res. Lett. 46, 1441–1448.